Paleoceanography and Paleoclimatology

RESEARCH ARTICLE
10.1029/2024PA004870

A Proxy System Modeling Approach to Combining Tree-Ring and Sediment-Based Paleotempestological Records

Elizabeth J. Wallace[1], Sylvia Dee[2], Joshua Bregy[3,4], and Kerry A. Emanuel[5]

[1]Department of Earth and Ocean Science, Old Dominion University, Norfolk, VA, USA, [2]Department of Earth, Environmental, and Planetary Sciences, Rice University, Houston, TX, USA, [3]Department of Environmental Engineering and Earth Sciences, Clemson University, Clemson, SC, USA, [4]Glenn Department of Civil Engineering, Clemson University, Clemson, SC, USA, [5]Lorenz Center, Massachusetts Institute of Technology, Cambridge, MA, USA

Abstract The short and biased observational record of tropical cyclones (TCs) limits scientific understanding of how these destructive storms respond to climate forcing. Paleohurricane records use natural archives (tree rings, coarse-grained sediment) to reconstruct TC properties (frequency and intensity of rainfall, wind) over the past few hundreds to thousands of years. However, different sensitivities and sampling biases in the various paleohurricane proxies restrict our ability to compile these records into regional or basin-scale TC estimates. Here we test how well pseudo tree-ring records of paleohurricanes capture TC rainfall and occurrence. Using a large set of statistically downscaled storms forced with the Max Planck Institute (MPI-ESM-P) model as boundary conditions for the past millennium, we generate a 1000-member ensemble of pseudo tree-ring records of latewood width from southern Mississippi using a Poisson process-based random draw. Pseudo records convert synthetic TC rainfall into latewood width using a previously published statistical calibration and seasonal sensitivity. We show that fourth quantile thresholds applied to pseudo latewood data successfully identify years with TC strikes. Comparing pseudo tree-ring records with pseudo sediment records from the Gulf Coast indicates promise in combining proxies sensitive to TC rainfall with proxies sensitive to storm overwash. Sediment records that are sensitive to lower intensity storms (≥Saffir Simpson Category 1) are more compatible with tree-ring records, suggesting a need for more of these low intensity threshold records in the Gulf to facilitate future multi-proxy efforts to reconstruct past TC properties.

Key Points:

- Applying quantile thresholds to latewood tree-ring records from the Gulf Coast identifies years with at least one tropical cyclone (TC)
- Low threshold paleohurricane sediment proxies strongly covary with tree ring proxies suggesting promise in future multiproxy comparisons
- We need a wider network of low-threshold sediment proxies combined with tree ring sites to reconstruct regional TC strikes

Supporting Information:

Supporting Information may be found in the online version of this article.

Correspondence to:

E. Wallace,
ejwallac@odu.edu

Citation:

Wallace, E. J., Dee, S., Bregy, J., & Emanuel, K. A. (2024). A proxy system modeling approach to combining tree-ring and sediment-based paleotempestological records. *Paleoceanography and Paleoclimatology*, *39*, e2024PA004870. https://doi.org/10.1029/2024PA004870

Received 6 FEB 2024
Accepted 30 AUG 2024

Author Contributions:

Conceptualization: Elizabeth J. Wallace, Sylvia Dee, Joshua Bregy
Data curation: Elizabeth J. Wallace, Kerry A. Emanuel
Formal analysis: Elizabeth J. Wallace, Joshua Bregy
Funding acquisition: Elizabeth J. Wallace, Sylvia Dee, Kerry A. Emanuel
Investigation: Elizabeth J. Wallace, Joshua Bregy
Methodology: Elizabeth J. Wallace, Sylvia Dee
Project administration: Elizabeth J. Wallace, Sylvia Dee
Resources: Sylvia Dee

1. Introduction

Tropical cyclones (TCs) are highly destructive natural disasters producing strong winds, intense rainfall, and storm surge that inundates coastlines and damages infrastructure (Pielke et al., 2008). Tropical cyclone precipitation (TCP), in particular, is one of the leading drivers of dangerous conditions, fatalities, and infrastructure damage during storms (Czajkowski et al., 2017; Rappaport, 2014). For example, Hurricane Harvey generated over 152 cm of rain in the Houston/Galveston Bay area in 2017. The storm ultimately cost over $125 billion dollars (Blake & Zelinsky, 2018), and many in Houston are still recovering from the losses. Recent work has shown that human induced climate change has increased the risk of anomalously high TC rainfall events like Hurricane Harvey (Emanuel, 2017; Risser & Wehner, 2017; Van Oldenborgh et al., 2017). Observations suggest that TC rain rate has increased globally, with more rain falling in the outer bands of TCs (Guzman & Jiang, 2021; Tu et al., 2021). Storms are stalling near the coast more often (Hall & Kossin, 2019) and decaying at a slower rate (Li & Chakraborty, 2020). In the North Atlantic, precipitation in major landfalling hurricanes has increased substantially (Touma et al., 2019).

While current and future TC rainfall patterns are well constrained, changes in TC *frequency* are not (Sobel et al., 2021). Ultimately, the rain-related risk associated with TC events is controlled by frequency, in that a storm cannot impart damages if it does not occur. Model projections of global TC frequency often differ *in sign* (Lee et al., 2020); some models show increased frequency (Bhatia et al., 2018), and some show decreased frequency (Sugi et al., 2017). Furthermore, the short observational (~170 years) and satellite records (~50 years) of TCs restrict our knowledge of how TC frequency and rainfall are modulated by decadal-to-centennial scale climate variability. Available observations show that storm tracks are modulated by long term climate modes like the North Atlantic Oscillation via steering winds (Kossin et al., 2010) and broadly, by Atlantic sea surface temperature (SST) patterns (Dare & McBride, 2011; Emanuel, 1999). El Niño-Southern Oscillation (ENSO) events also affect TC formation and growth, with La Niña (El Niño) spurring more (fewer) storms in the North Atlantic

Software: Elizabeth J. Wallace, Joshua Bregy, Kerry A. Emanuel
Supervision: Sylvia Dee
Validation: Elizabeth J. Wallace
Visualization: Elizabeth J. Wallace
Writing – original draft: Elizabeth J. Wallace, Sylvia Dee, Joshua Bregy
Writing – review & editing: Elizabeth J. Wallace, Sylvia Dee, Joshua Bregy, Kerry A. Emanuel

(Gray, 1984; Klotzbach et al., 2017; Patricola et al., 2014). However, the feedbacks between these nonlinear modes of climate variability and TC properties are still uncertain due to the scarcity of observations over the 20th century.

To address this, we can use paleohurricane proxies to supplement our observations and extend the record of TC events back hundreds to thousands of years. The vast majority of paleohurricane records use sediment (Oliva et al., 2018; E. J. Wallace, Dee, et al., 2021) or tree (Bregy et al., 2022; Miller et al., 2006; Trouet et al., 2016) cores. Sediment cores record the temporal evolution (frequency) of landfalling TC events. During TCs, high wind and wave action mobilize coarse-grained sediment, which subsequently is deposited in various environments, including coastal ponds/lagoons (Donnelly et al., 2015; Donnelly & Woodruff, 2007; Rodysill et al., 2020) or blue holes (Schmitt et al., 2020; E. J. Wallace et al., 2019; E. J. Wallace, Donnelly, van Hengstum, Winkler, McKeon, et al., 2021; Winkler et al., 2020). Tree cores record climate changes at monthly to-annual resolution (Tucker & Pearl, 2021). In particular, latewood width (the section of a tree ring that grows during the hurricane season) in longleaf pine (*Pinus palustris,* Mill.) is strongly linked to the short duration and high volume precipitation produced by TCs (P. A. Knapp et al., 2016, 2021; Maxwell et al., 2021). Rain from TCs infiltrates quickly through the sandy soils and gentle topography near the coast reaching/raising the water table depth. During these storms, the shallow lateral roots of longleaf pine species can access storm-related rainwater (Montpellier et al., 2020). A recently published record from De Soto National Forest calibrated the width of the latewood portion of tree rings from longleaf pine to TC precipitation data over the same region (Bregy et al., 2022).

To resolve TC climate signals, there has been a push toward compiling reconstructions from neighboring sites (e.g., E. J. Wallace, Donnelly, van Hengstum, Winkler, Dizon, et al., 2021). Both sediment-based and tree-ring based records are biased. Sediment records are sensitive only to intense TCs (≥Category 3) that pass nearby (>200 km) (E. J. Wallace, Dee, et al., 2021). These biases make it more likely that an individual sedimentary paleohurricane record captures random variability in TCs rather than climate variability (E. J. Wallace et al., 2020). Tree ring records, on the other hand, are biased toward the rainiest storms. The relationship between TC precipitation and TC frequency is uncertain. Years with more frequent TCs will likely have more TC rainfall, but this relationship can be complicated by other TC properties that produce more rain (i.e., translational velocity, (Hall & Kossin, 2019),). In addition, there is no way to isolate the role of TCs in producing latewood growth bands in trees compared to other storm systems (e.g., thunderstorms, extratropical cyclones). Until there is a direct relationship established between TCP and TC frequency, it is difficult to compare sediment data with tree core data.

In order to reconstruct a basin-wide or regional TC climate signal, we need large networks of paleohurricane proxy data (E. J. Wallace, Dee, et al., 2021; E. J. Wallace & Dee, 2022). At present, with sedimentary or tree-ring proxies in isolation, we are limited in our ability to reconstruct basin-scale or regional TC trends over time (E. J. Wallace, Dee, et al., 2021). Integrating across proxy types in these locations can fill gaps in paleohurricane networks, yet to date, no work has been done to integrate sedimentary paleohurricane records with tree-ring proxies. This is due to challenges related to combining estimates of direct TC occurrence (sourced from sediment proxies) with TC-related climate properties (e.g., rainfall estimates sourced from tree-ring proxies).

To address this problem, here, we explore uncertainties in tree-ring reconstructions of TCP and frequency and their combination with sediment proxies using a pseudo proxy forward modeling approach. Proxy system models are widely used to explore uncertainties in proxy interpretation and to link climate model data to proxies in common units (Dee et al., 2015; Evans et al., 2013). Pseudo proxy approaches have been successfully applied to assessing uncertainties in sediment-based paleohurricane records (Wallace et al., 2020). Scaling up from the individual records, pseudo proxies have also been used for sensor placement recommendations and network optimization for paleohurricane records in the North Atlantic (E. J. Wallace, Dee, et al., 2021). Building from these and other studies, we use a large data set of synthetic TCs to generate the first pseudo tree-ring latewood records from the Gulf Coast. We compare the pseudo-proxy data to actual proxy data including a reconstruction from longleaf pine in De Soto National Forest in Mississippi (Bregy et al., 2022). We explore key questions related to merging paleohurricane proxies of different types by comparing our pseudo tree ring record to idealized pseudo sediment records generated in the same region. These questions include: (a) Can tree-ring proxies years when TCs occur? and (b) Can tree-ring records of TCP be related to sediment records of TC occurrence for a given location?

2. Data and Methods

The pseudo proxy approach used here follows three steps. First, we generate large numbers of synthetic TCs using a statistical/dynamical TC model (Emanuel et al., 2008) driven by a fully forced past millennium simulation from the Max Planck Institute Earth System Model (MPI-ESM-P). Second, we generate pseudo tree-ring and pseudo sediment records using the properties of these storms (intensity and derived precipitation) that are captured in natural archives. Third, all pseudo records are compared to each other as well as observational and proxy data. Details on our methods for each step in this process are given below.

2.1. The Synthetic Tropical Cyclone Data Set

Building a pseudo record of extreme events (like TCs) requires simulating large numbers of extremes to allow for robust statistical analyses. The observational record often includes only a small number of extremes impacting a given location. In our case, only 45 TCs have passed over De Soto National Forest since the beginning of rain gauge measurements (~1948 CE) (K. Knapp et al., 2010).

We simulate 57,800 TCs (50 storms/year) passing within 223 km of De Soto National Forest (31.08°N, 89.08°W) over the past millennium using a statistical/dynamical TC model (Emanuel et al., 2008). Synthetic TCs range from tropical storms to Category 5 hurricanes in intensity. The 223 km radius represents the average radius of closed isobar for observational storms (Matyas, 2010) and allows us to include only storms that are likely to generate rainfall at our site. The statistical/dynamical model used here spins up storms from background climate conditions sourced from the MPI-ESM-P last millennium (850–1850 CE) and historical simulations (1851–2005 CE) (Giorgetta et al., 2013). The storm generation methods are summarized in Text S1 in Supporting Information S1.

Rainfall over the lifetime of each synthetic storm is generated using a tropical cyclone rainfall (TCR) algorithm (Zhu et al., 2013). Details on the algorithm can be found in Zhu et al. (2013) and Lu et al. (2018), and are summarized in Text S1 in Supporting Information S1. The TCR model is computationally efficient and can help characterize TC rainfall climatology (Feldmann et al., 2019) and make risk assessments (Emanuel, 2017). While the TCR model cannot capture individual convective systems, it can simulate intense eyewall convection and capture precipitation outside the storm core (Zhu et al., 2013). TCR model output accurately simulates existing observations of storm rainfall (Feldmann et al., 2019). For this study, we extract total storm precipitation (in mm) at our De Soto tree core site for each of the 57,800 synthetic storms in our data set. Precipitation amounts per storm range from 0 to 1932 mm.

2.2. Observational Data Products

We compare our synthetic TC data to two observational products for validation: (a) The International Best Track Archive for Climate Stewardship (IBTrACS; K. Knapp et al., 2010) and (b) the TC Precipitation Data set (TCPDat; Bregy et al., 2020). The IBTrACS data set provides the position and intensity of TCs in the North Atlantic from 1851 to present. The most reliable portion of this data set extends over the satellite era from 1974 onwards and decreases in accuracy and completeness moving further back in time; the era prior to aircraft reconnaissance (pre-1944) contains the largest biases (Emanuel, 2003).

We extract observational TCP data from TCPDat at De Soto National Forest (31.08°, −89.08°). TCPDat (Bregy et al., 2020) is a $0.25° \times 0.25°$ data set of TC precipitation for the continental USA from 1948 to present. This data set extracts daily precipitation associated with observational TCs from a unified rain gauge data set (the Climate Prediction Center Unified Precipitation data set (CPC URD (Higgins et al., 2000)). TCPDat offers a spatially consistent view of TCP but is known to underestimate the magnitude of TCP (Bregy et al., 2020).

2.3. From TCs to Latewood Width of Longleaf Pine

We generate an ensemble of pseudo latewood records by modifying previously published methods for generating pseudo sediment records (E. J. Wallace et al., 2020). Briefly, we generate 1,000 records of storm occurrence by randomly drawing an integer number of storms (x) from the 50 storms available for each year of climate. A Poisson random draw determines x using the annual storm frequency (λ) from the model for that year (0.17 TCs/year to 1.36 TCs/year). Across our 1,000 records, x ranges from 0 to 8. This method creates 1,000 different

realizations of storms striking southern Mississippi over the past millennium with different numbers of and different actual storms occurring in each realization.

To move from storm occurrence to a pseudo tree-ring reconstruction, we apply a published linear regression reconstruction model presented in Bregy et al. (2022). This reconstruction model was built by running a linear regression of July–September TCP totals (from the rain-gauge-based observational product TCPDat (Bregy et al., 2020)) onto the De Soto latewood width data. Details on the De Soto National Forest latewood data can be in Bregy et al. (2022) but are summarized below. Longleaf pine samples from De Soto National Forest were collected from living trees, stumps, and archeological samples and latewood ring widths were measured. Samples were detrended using a two-thirds smoothing spline. The 2/3 smoothing spline method removes biological and non-climatic growth while preserving low-frequency variability (Cook & Peters, 1981). Adjusted latewood ring width values showed a much stronger correlation (r = ~0.6) with TCP than non-TCP (r = ~0.4) (Bregy et al., 2022).

Since latewood growth in longleaf pine occurs from July to September (P. A. Knapp et al., 2021; Maxwell et al., 2021), we limit our synthetic TC data to only events occurring in these months. For each year in each pseudo record, we sum precipitation across each storm to reach an annual precipitation amount at the site from TCs only (Figure 1). This precipitation total is a function of both the amount of precipitation in each storm and the frequency of storms passing over the site in that year. Annual precipitation is then converted into latewood width using Equation 1 (Bregy et al., 2022):

$$\mathrm{LWa} = \frac{\mathrm{TCP} + 67.01}{94.04} + \varepsilon \quad (1)$$

where TCP is annual TC precipitation in mm, LWa is adjusted latewood width in mm, and $\mathcal{E}$ is a white noise error term. The linear relationship in Equation 1 is temporally stable and captures 40% of the variance in seasonal TCP totals (Bregy et al., 2022). Equation 1 is only calibrated over the observational period (1948–2012). Linear regression reconstructions bias results toward the mean, so Equation 1 tends to overestimate latewood widths when TCP is low and underestimate TCP totals for the most extreme events. We introduce an error term to the calibration equation to account for inherent uncertainties in the calibration (Equation 1).

We convert from latewood width to TC frequency (Figure 2a) using our pseudo tree-ring records. Years with simulated latewood widths in the fourth quartile (Q4, 40.07 mm) are counted as years where a storm made landfall according to the pseudo tree core. To analyze event frequency patterns, we apply a 50-year moving sum to our Q4 frequency data as is standard practice in paleotempestology studies (Bregy et al., 2022).

2.4. From TCs to Coastal Overwash Sediment Signatures

Storms raining over De Soto National Forest can also create storm surge along the Gulf Coast. These high waves can produce overwash signatures in coastal lakes which are proxies of storm occurrence (Brandon et al., 2013; Lane et al., 2011; Rodysill et al., 2020). Compiling sediment proxies of TC occurrence with tree ring proxies of TC rainfall requires testing whether these proxies record the same or similar populations of storms. Therefore, we create a theoretical framework for testing whether our synthetic data set of TC rainfall could translate into overwash at the coastline.

We create pseudo sediment records using our 1,000 records of storm occurrence from De Soto National Forest. We find the geographic location where each track in the data set intersects the coastline and the intensity of that storm as it makes landfall (Figure 1b). Existing paleohurricane records from the Gulf Coast are either low-threshold records (capture ≥ Category 1 storms; Brandon et al., 2013; Lane et al., 2011) or high-threshold records (capture ≥ Category 3 storms; Bregy et al., 2018; K. Liu & Fearn, 2000). Therefore, only storms with landfall intensities ≥ Category 1 (64 knots) and ≥Category 3 (96 knots) leave a deposit in our low-threshold and high-threshold pseudo records, respectively. We assume each record has a minimum sedimentation rate of 1 cm/year such that each sediment record can only distinguish if at least one storm made landfall each year. If two or more storms with high enough intensity occur each year, only one indicator layer is created. Throughout this analysis, we assume availability of coastal basins appropriate for capturing overwash layers at every place our synthetic storms make landfall. Both our assumptions (i.e., one cm/year sedimentation rate and ample availability of coastal basins along the Gulf Coast) do not reflect reality but allow us to test an optimal scenario. Our approach is motivated by the

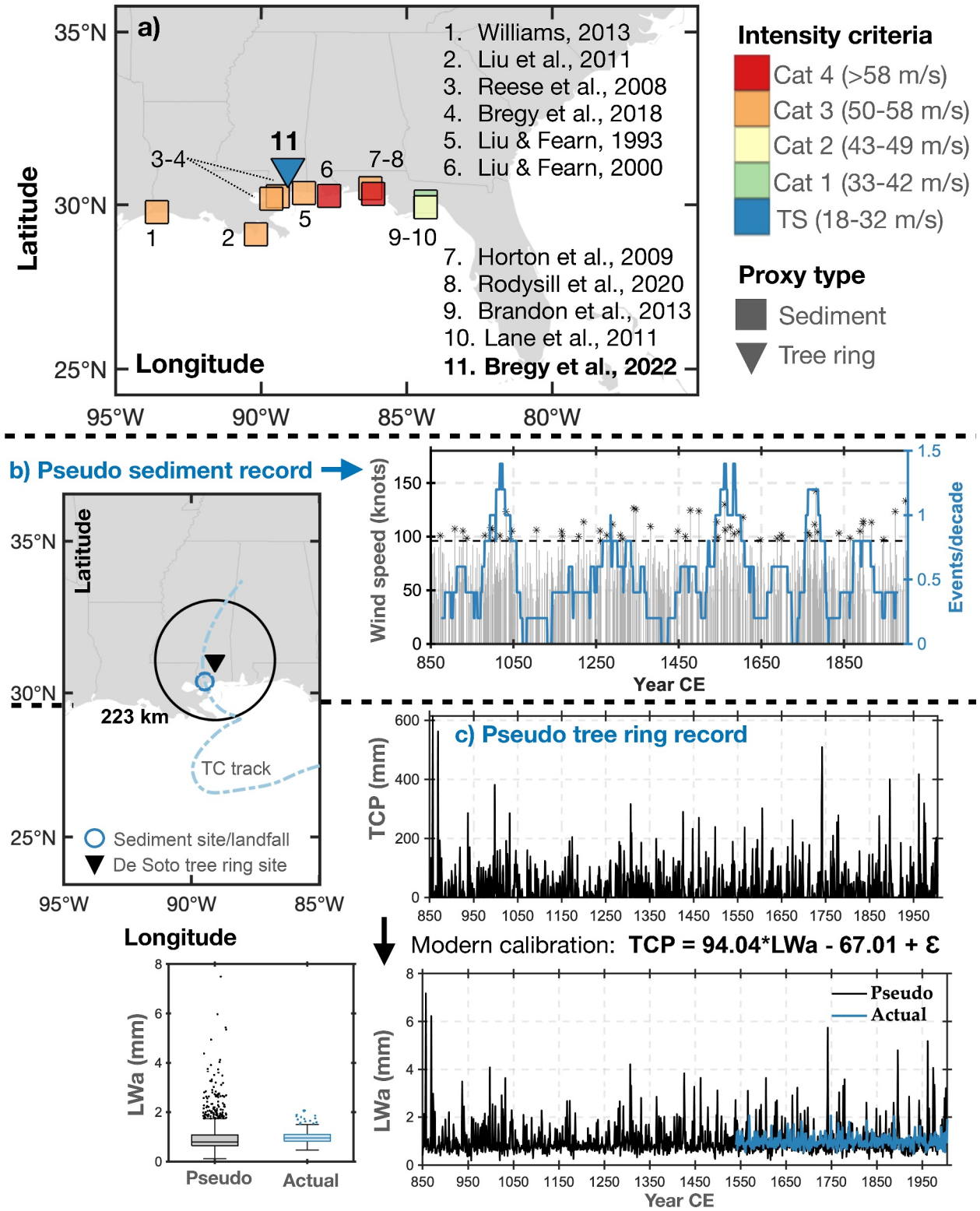
a)
1. Williams, 2013
2. Liu et al., 2011
3. Reese et al., 2008
4. Bregy et al., 2018
5. Liu & Fearn, 1993
6. Liu & Fearn, 2000
7. Horton et al., 2009
8. Rodysill et al., 2020
9. Brandon et al., 2013
10. Lane et al., 2011
11. Bregy et al., 2022
Intensity criteria
Cat 4 (>58 m/s)
Cat 3 (50-58 m/s)
Cat 2 (43-49 m/s)
Cat 1 (33-42 m/s)
TS (18-32 m/s)
Proxy type
Sediment
Tree ring
Latitude
Longitude
35°N
30°N
25°N
95°W
90°W
85°W
80°W
b) Pseudo sediment record
223 km
TC track
Sediment site/landfall
De Soto tree ring site
Wind speed (knots)
Events/decade
Year CE
c) Pseudo tree ring record
TCP (mm)
Modern calibration: TCP = 94.04*LWa - 67.01 + Ɛ
LWa (mm)
Pseudo
Actual

Figure 1.

idea that if the results suggest that it is possible to relate TC rainfall proxies to TC overwash proxies in this idealized scenario, future efforts can assess the practicality of obtaining such measurements.

Each of our pseudo tree-ring and pseudo sediment records provide an estimate of years with TC strikes at a given location over the past millennium. To determine whether sediment and tree-ring records document the same storm year patterns, we perform correlation analyses between our estimates of TC frequency produced by our different pseudo records.

2.5. Data Model Comparison: Spectral Analysis

We compare our pseudo records to the real published latewood data to assess how well our synthetic records capture real TCP variability. We estimate the power spectra of the 1,000 pseudo records of latewood width data and real latewood width data using Thomson's multi-taper method (Thomson, 1982). Since annual TCP is related both to TC frequency and TC rainfall, we also calculated power spectra for synthetic TC frequency and mean annual TCP over the past millennium. We normalize all data prior to spectral analysis. To isolate significant spectral peaks across time series, we calculated the power spectra of an autoregressive [AR(1)] model forced by white noise and with realistic autocorrelation matching our pseudo records (Ault et al., 2013). Peaks in power spectra exceeding the 95% confidence level of our AR(1) null hypothesis are considered significant.

2.6. Properties of the Rainiest Storms

Paleotempestology proxy reconstructions do not permit investigation of storm properties that leave indicator layers, but with pseudo proxies, all environmental conditions are known. We use our pseudo latewood records to analyze the characteristics of the rainiest storms that contribute to larger latewood width growth years in De Soto National Forest. It is unclear whether Q4 latewood ring width signatures in De Soto longleaf pine trees are biased toward certain kinds of TCs. We analyze the sinuosity, the intensity at the time of closest passage, translational speed, direction of passage (east or west of site), and genesis region of synthetic storms generating the 99th, 95th, and 75th percentile (Q4) peaks in annual TCP/latewood width across our pseudo records. These criteria are chosen because many of these TC properties impact TCP in observed storms (Matyas, 2010; Touma et al., 2019; Yu et al., 2017). We define storm sinuosity as the total meandering distance of cyclone travel divided by the vector length between the start and finish location (Terry & Feng, 2010). Translational velocity is defined as the average speed of the TC as it travels within a 3° box of the site. All speeds were calculated as the distance between two hourly points on a track divided by the time between points (i.e., 2 hr). Direction of passage is denoted as either east or west given that storms passing through southern Mississippi are typically southerly moving either to the east or west of our tree ring site (Figure 1b). TC genesis density is calculated as the number of TC starting points per 0.5° × 0.5° box per year.

3. Results

3.1. Data Model-Comparison: Latewood Records

Pseudo tree-ring records generated using MPI synthetic TCP show similar mean latewood widths (1.04 mm) to the real De Soto paleo archive (0.99 mm). However, the variance in pseudo latewood widths (0.47 mm) is over seven times larger than the variance in real latewood width (0.06 mm) (Figure 1c). To understand the discrepancy in latewood width variance, we examined individual properties of the MPI synthetic TCs, most of which compare favorably to the observations. Genesis locations, track trajectories, and storm max intensity all broadly match observations within uncertainties (Figures 3a–3d). The differences between our large synthetic TC data set (7,750 storms from 1851 to 2005 CE) and the smaller observational data (121 storms from 1851 to 2005 CE) arise in part

Figure 1. (a) Gulf of Mexico paleohurricane sites (Brandon et al., 2013; Bregy et al., 2018, 2022; Horton et al., 2009; Lane et al., 2011; K.-B. Liu & Fearn, 1993, 2000; K.-B. Liu et al., 2011; Reese et al., 2008; Rodysill et al., 2020; Williams, 2013) by proxy type (shape) and intensity criteria (color). (b) Example high-threshold pseudo sediment record. Map shows a synthetic tropical cyclone (TC) making landfall. Intensity at landfall for all storms occurring is shown over the last millennium (gray bars). TCs that leave a deposit (intensity ≥96 knots) are shown as black stars. The 50-year window event frequency is plotted (blue). (c) Pseudo latewood records start with accumulated Tropical cyclone precipitation (TCP) at De Soto National Forest (31.08°N, 89.08°W) from all TCs that pass within a 223 km circle. TCP is converted into adjusted latewood widths using a published calibration equation (Bregy et al., 2022). An example pseudo latewood record (black) is compared to the real latewood measurements (blue) (Bregy et al., 2022). Boxplots show the median (center line), interquartile range (box), and outliers (dots) for a single pseudo record (black) compared to the real latewood proxy (blue).

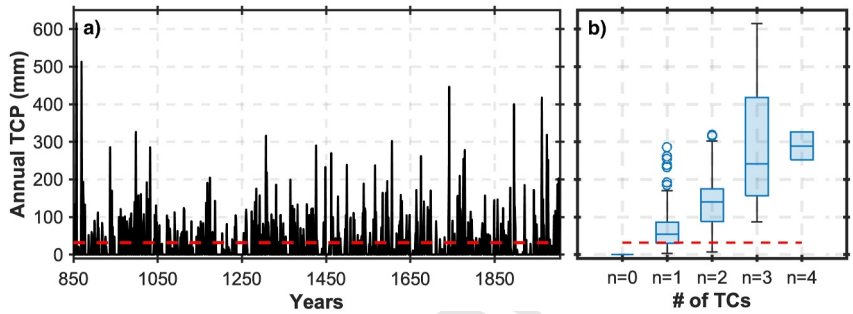

Figure 2. (a) Randomly selected example pseudo record of JAS tropical cyclone precipitation from 850 to 2005 CE. The fourth quantile threshold (40.08 mm) is shown (red dotted line). (b) Box plot of annual precipitation as a function of the number of storms that occurred in each year. Boxplots show the median (center line), interquartile range (box), and outliers (dots) for all 1,000 pseudo records.

from the smaller sample size and observing biases toward landfalling and higher intensity storms (e.g., Landsea & Franklin, 2013; Vecchi & Knutson, 2011; Villarini et al., 2011) associated with the instrumental record.

Thus, the larger variance created in the pseudo records arises from higher variance in both synthetic TC rainfall and TC frequency. Storm total accumulated precipitation in MPI synthetic storms is much higher than observational storms extracted from TCPDat (Figure 3e). Our TC rainfall algorithm downscaled from reanalysis data matches rain gauge and radar data well (Feldmann et al., 2019). Therefore, this pattern of rainier storms in the model likely arises from a combination of biases in our observational product (TCPDat) and our climate model (MPI-ESM). First, TCPDat, which applies a conservative search radius (223 km) for storm rainfall, is built to underestimate rainfall amounts over the lifetime of a storm (Bregy et al., 2020). Second, observational rain gauge data is inherently biased toward capturing less storm rainfall. Most gridded gauge data sets undergo interpolation and do not capture individual extreme events well (Ensor & Robeson, 2008). The return period of storm rainfall calculated using radar data from Feldmann et al. (2019) matches our synthetic storms much better than return periods calculated using TCPDat (gauge data) (Figure S1 in Supporting Information S1). Unfortunately, radar data rarely spans greater than a 30-year observational period which makes it less suitable for paleo comparisons than the >90-year observational period of gauge data (Feldmann et al., 2019). On the other hand, the MPI-ESM simulations are biased toward warmer temperatures over the U.S. Gulf Coast (Giorgetta et al., 2013). These warm biases in the model generated a longer tail for the distribution of synthetic storm rainfall (Figure 3e).

These outliers in TCP produce unrealistic extremes in both latewood width and precipitation amounts in our pseudo records (Figure 1c). These biases prevent comparison of patterns in TCP amounts over the past millennium. For this paper, we focus our analyses on TC properties inferred from latewood records that are not related to TCP magnitude, including storm frequency and spectral properties.

Our pseudo tree-ring records show similar spectral properties to the real De Soto latewood width record (Figure 4a). Both records show substantial high-frequency variability with significant spectral peaks in the 3–7-year band associated with El Niño–Southern Oscillation (ENSO) (Diaz & Pulwarty, 1994). Both real and pseudo tree-ring records show little low-frequency variability with few to no significant spectral peaks exceeding 25 years (Figure 4c). This spectral shape matches the shape of synthetic TC frequency but not synthetic TC rainfall: TC frequency similarly lacks low-frequency variability, while synthetic rainfall shows significant variability in the 100-year and greater ranges of the spectrum. Both frequency and rainfall vary significantly in the ENSO band (3–7 years) (Figure 4b).

3.2. Converting TC Rainfall Proxy to TC Frequency

The conversion from TC rainfall captured by latewood records into TC frequency metrics is uncertain. Dendroclimatology records typically assume that fourth quantile (Q4) peaks in latewood width serve as a metric of TC frequency. We explicitly test this assumption using our pseudo records and find a strong correlation between frequency of Q4 latewood events and the frequency of JAS storms (Figure 5b, mean rho of 0.75 from 1,000 pseudo records). Across all 1,000 pseudo records, we find that using a Q4 cutoff of 40.08 mm of rain reliably extracts years with at least one storm (Figure 2b). Daily background precipitation values in MPI are rarely above the Q4 threshold.

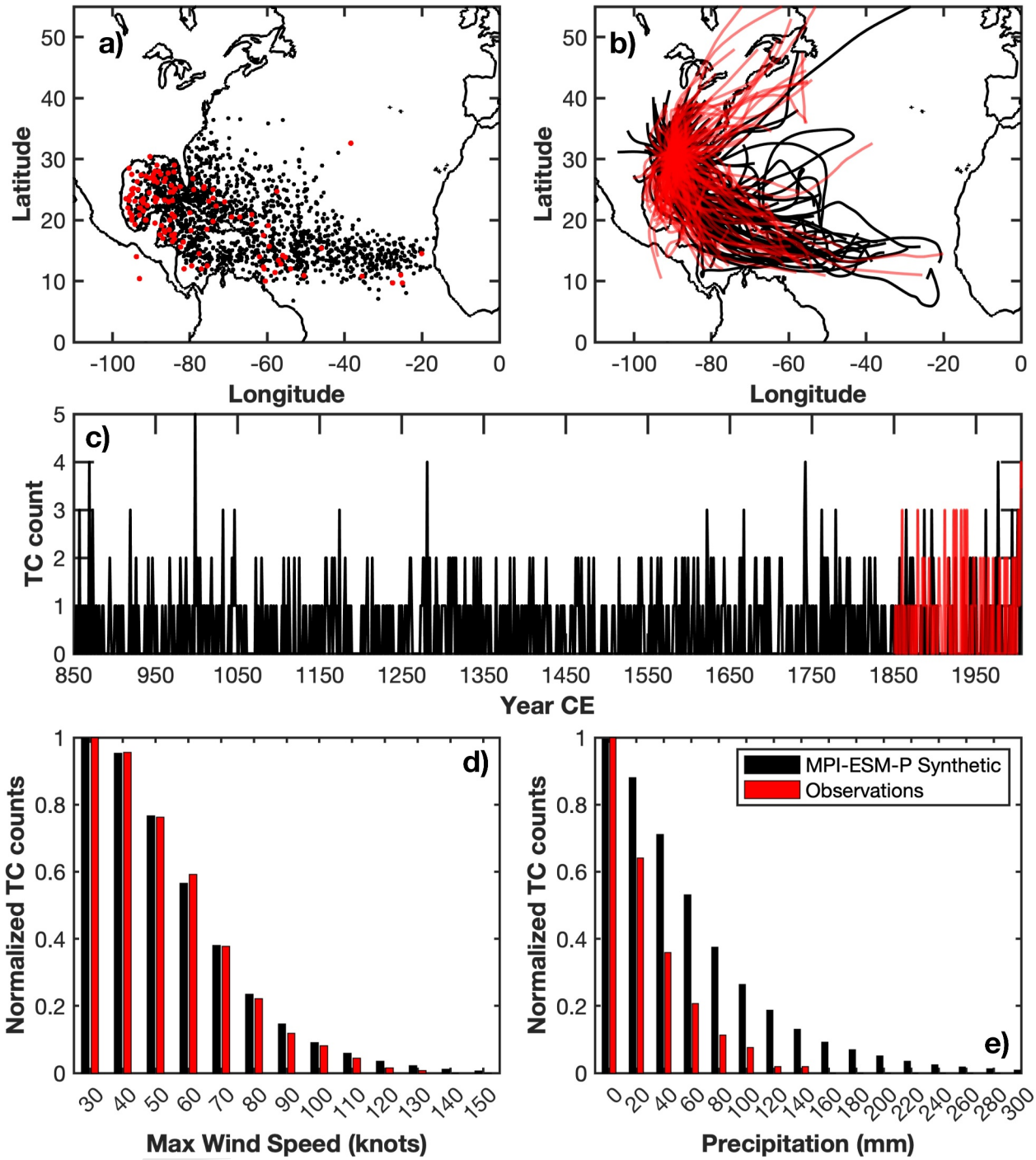

Figure 3. (a) Genesis points for 121 observed tropical cyclones (TCs) (red) compared to 1,800 randomly selected MPI synthetic TCs (black) that occurred from 1851 to 2005 CE. (b) 100 randomly selected synthetic (black) and observed (red) tracks from 1851 to 2005. (c) Average TC frequency per year, (d) distribution of maximum sustained wind speed and (e) total accumulated storm precipitation (in mm) for observed (red) and synthetic storms (black) in the North Atlantic. The TC counts in panels d and e are normalized by the total number of storms in each data set. All synthetic storms were generated by a statistical downscaling model (Emanuel et al., 2008). All observed storms were drawn from the IBTrACS database (K. Knapp et al., 2010). Observed TC rainfall in panel e is drawn from rain gauge data compiled in TCPDat (Bregy et al., 2020).

In fact, only 39 of 106,352 daily background MPI precipitation values (0.037%) from the past millennium are above the Q4 cutoff (Figure 6). The Q4 cutoff, however, cannot distinguish between years with one storm and more than one storm (Figure 2b). This limitation is common to all paleohurricane proxies, though, and should not pose a

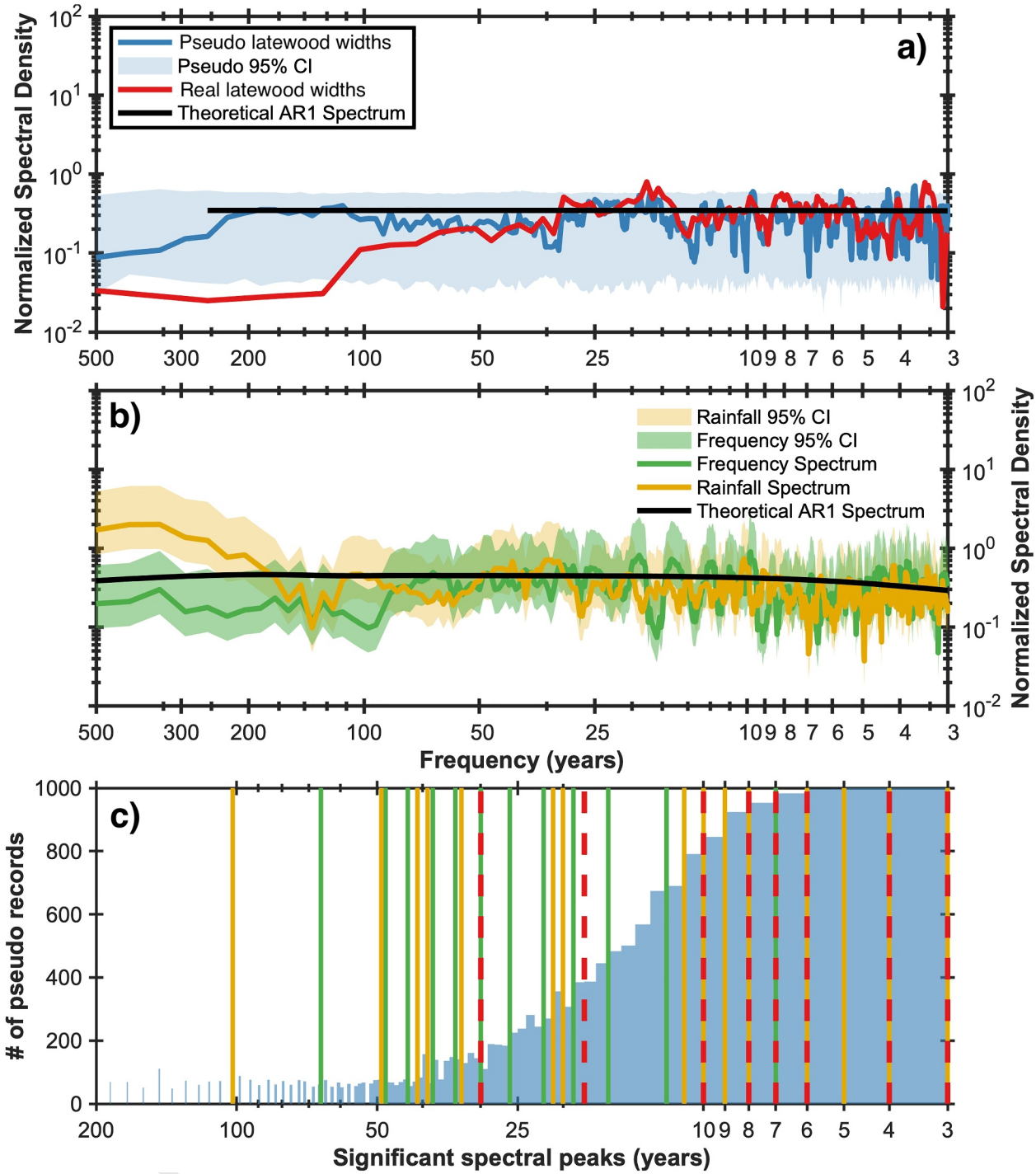

Figure 4. (a) Normalized spectral density of an example pseudo latewood width record (blue) compared to real latewood width data (red) (Bregy et al., 2022). (b) Normalized spectral density of average annual MPI-ESM synthetic tropical cyclone (TC) precipitation (yellow) compared to MPI TC frequency (green). In both panels, 95% confidence intervals (shaded regions) and a theoretical AR1 spectrum (black) are shown. (c) Histogram of the number of pseudo records that exhibit significant spectral density peaks in each frequency band. Significant spectral peaks for synthetic TC frequency, TC rainfall, and the real latewood width data are overlain in green, yellow, and red, respectively.

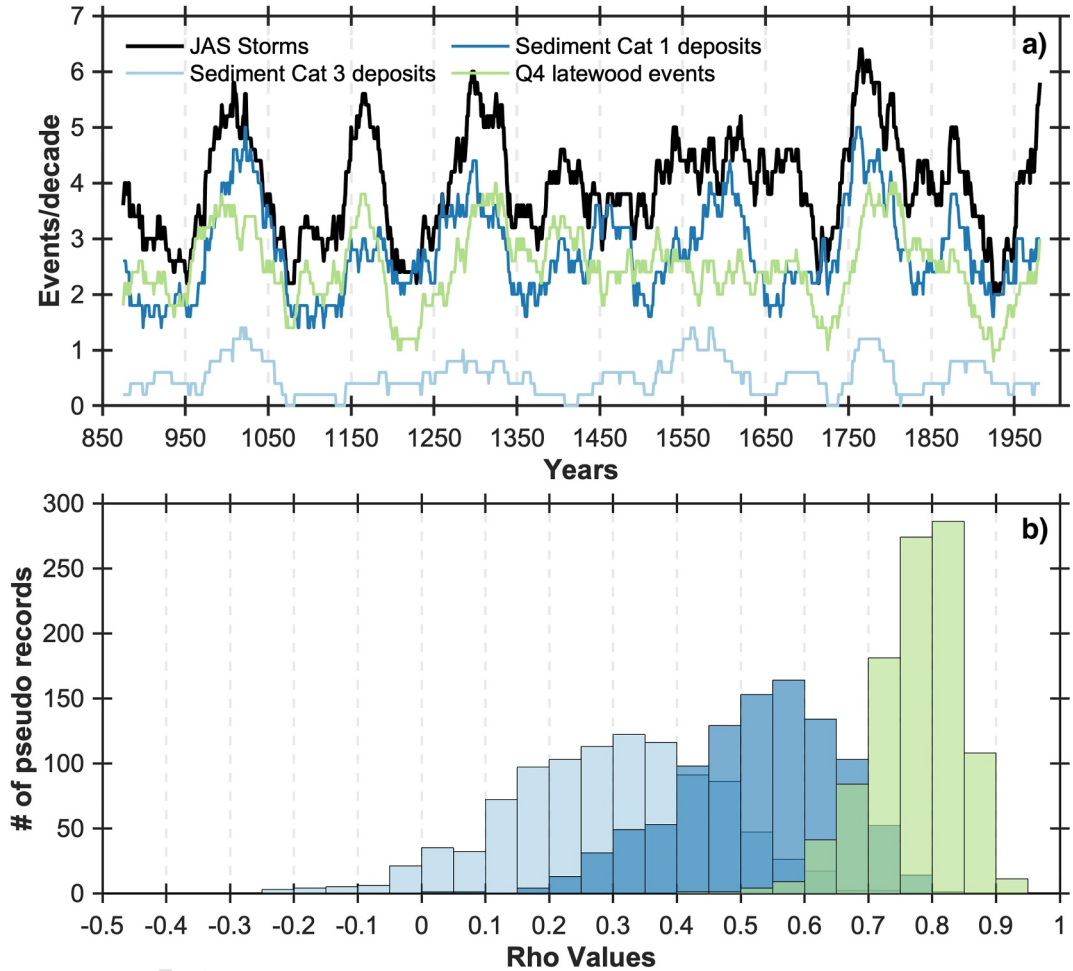

Figure 5. (a) Randomly selected example pseudo record 50-year moving window event frequency for July–September (JAS) storms (black), fourth quantile (Q4) latewood width events (green), HT (Category 3 and above) sediment deposits (light blue), and LT (Category 1 and above) sediment deposits (dark blue). (b) Histogram of the correlation coefficients between JAS storms and Q4 latewood events (green), Q4 latewood events and LT sediment deposits (dark blue), and Q4 latewood events and HT sediment deposits (light blue) by number of pseudo records.

problem for multiproxy comparison. For example, sediment records of storm overwash are also unable to distinguish between multiple storms making landfall in a year (D. J. Wallace et al., 2014).

Given that quantile thresholds can successfully identify storm frequency using latewood growth data, we can explore whether multiproxy comparisons on tree ring records and sediment records are possible. Paleohurricane sediment records can only be combined with tree ring records if the storms that are rainy enough to impact tree growth are also intense enough at the coastline to generate surge. In our case, we tracked the intensity at landfall of each of the 57,800 synthetic storms that rained over De Soto National Forest (Figure 1b). Many of the storms that were identified using the Q4 cutoff in our pseudo tree-ring records were not categorized as a major hurricane on landfall (max wind speeds ≥96 knots). Approximately 10% of Q4 rainfall storms are major hurricanes (≥Category 3) at landfall while ∼50% of Q4 rainfall storms are hurricane strength (≥Category 1) at landfall. There is a significant correlation between the frequency of hurricane landfalls and pseudo latewood records (Figure 5b; $r = 0.52$, mean r across 1,000 records). The correlation between the frequency of major hurricane landfalls and Q4 rain events is still significant but much weaker (Figure 5b; $r = 0.30$, mean r across 1,000 records). These results suggest that even the rainiest storms at De Soto National Forest would not necessarily create coarse-grained overwash layers in coastal basins, especially those basins sensitive to overtopping under major hurricane conditions (e.g., Bregy et al., 2018; K. Liu & Fearn, 2000; Rodysill et al., 2020).

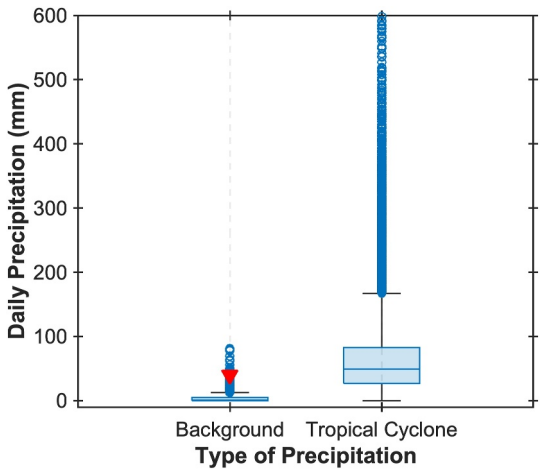

Figure 6. Boxplot of background daily rainfall totals (mm) in July–September from MPI-ESM-P simulations of past millennium and historical (850–2005 CE) compared to rainfall totals in MPI synthetic tropical cyclones run over the same time frame. Daily precipitation in the model is rarely larger than the Q4 cutoff (40.08 mm, red triangle).

3.3. Analysis of the Rainiest Storms

Using our synthetic storms, we tracked the properties of Q4 storms captured by our pseudo latewood records. We found a strong relationship between the closest distance of storm passage and rainfall at the De Soto National Forest site. Most storms (82%) that generated fourth-quartile rainfall passed within 150 km of the site (Figure 7a). Similarly, we also found that TCs that passed to the west of the site rain more (Figure 7e). Most TCs hitting Mississippi are moving in a northerly direction from the Gulf of Mexico. Therefore, De Soto National Forest experiences the most rain from the front right quadrant of a storm when it passes on the west side. TCP observations support this pattern finding maximum rainfall in the front quadrants of TCs with Atlantic TCs showing the most precipitation in the front right quadrant (Burpee & Black, 1989; Didlake & Kumjian, 2018; Lonfat et al., 2004).

Storm properties like intensity, sinuosity, and translational velocity created less clear relationships. There was no significant difference in the intensity of storms that generated fourth quantile rain accumulation (average intensity: 70 knots) compared to all events (average intensity: 67 knots). However, 99th percentile events were substantially more intense (average intensity: 113 knots). There is no difference in the sinuosity of storm tracks for rainy events versus all events (Figure 7c). The mean translational velocity of rainier storms is smaller than all events (Figure 7d). Fourth quantile events had an average translational velocity of 6.74 m/s compared to all events at 7.60 m/s. On average, events in the 99th percentile were almost 3.8 m/s slower than all events.

Most storms that pass within 223 km of De Soto National Forest form either in the Gulf of Mexico or in the Main Development Region (MDR: 10–20°N, 80–20°W). This is true in both the MPI synthetic data set and observations. We do not find strong relationships between storm genesis location and storm rainfall. Only the rainiest storms (99th percentile events) seem to preferentially form in the MDR before making landfall along the Gulf coastline (Figure 7f). These events are more intense and rainier, as they take longer to move through favorable oceanic conditions in the tropics before making landfall. On the other hand, storms forming in the Gulf of Mexico make landfall shortly after formation and have less time to develop into fully fledged storms.

4. Discussion

In paleotempestology, compilations are quickly being established as an important method for constraining TC climate shifts and robustly integrating proxy data with TC model output (Wallace & Dee, 2022; Yang et al., 2024). Ideally, these compilations will use the complete paleohurricane proxy network and integrate different types of proxies (e.g., trees, sediments). This paper represents proof of concept work that tests the practicality of using latewood width in coastal trees to reconstruct TC statistics (e.g., rainfall, years with TCs) and build multiproxy compilations. In this section, we use our analyses to offer suggestions for improving paleohurricane tree core proxies and making regional multiproxy paleohurricane compilations a possibility (Figure 8).

Sediment paleohurricane proxies record changes in TC landfalls; therefore, we tested whether thresholding of tree ring proxies of TCP (e.g., latewood width) can successfully capture years with TCs. Using synthetic storm climate for the past millennium and a published calibration between TCP and latewood width, we constructed an ensemble of pseudo records with similar mean values and spectral properties as real tree ring data from the Gulf Coast. Setting a fourth quantile threshold to our pseudo latewood data provided an estimate of TC occurrence that is strongly and significantly correlated with real occurrence (Figure 5b). Our work highlights that current approaches to reconstruct years with TC strikes using latewood growth bands have promise. We demonstrate a strong relationship between the amount of rain recorded each year in a latewood record and the occurrence of at least one storm (Figures 2b and 6). However, we were unable to distinguish whether one storm or many storms rained on a site each year using latewood width data alone.

A tree-ring record's inability to distinguish between years with one storm versus years with more than one storm does not pose a problem for future compilation efforts with sediment records. Even the highest resolution (i.e.,

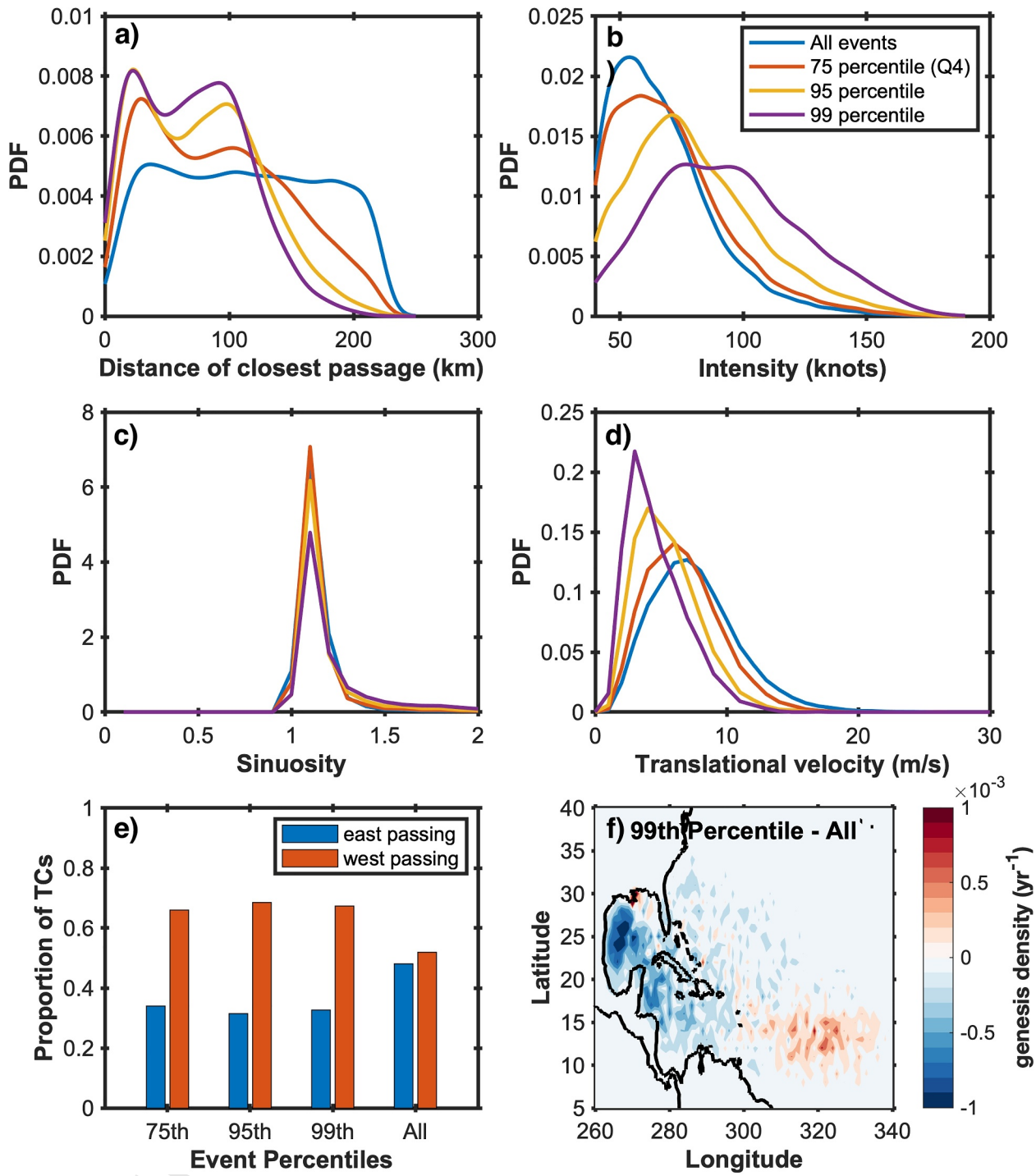

Figure 7. Probability distribution functions of tropical cyclone (TC) distance of closest passage (a), max wind speed (b), sinuosity (c), and translational velocity (d) for fourth quantile (75th percentile) rainfall (red), 95 percentile rainfall (yellow), 99th percentile rainfall (purple) and all (blue) TC events. (e) Histograms of the proportion of 75th, 95th, 99th, and all TC events in the synthetic data set that pass De Soto National Forest to the east (blue bar) versus the west (red bar). (f) Anomaly map of the genesis density for 99th percentile rainfall TC events compared to all TC events.

annual) paleohurricane sediment records also suffer from this bias. Annual sediment archives with one cm/year sedimentation rates can only distinguish whether at least one storm passed by a site in a year (E. J. Wallace et al., 2019; Winkler et al., 2022). Since both proxies have similar biases, researchers would not need to bias correct either proxy before integrating them into a single estimate.

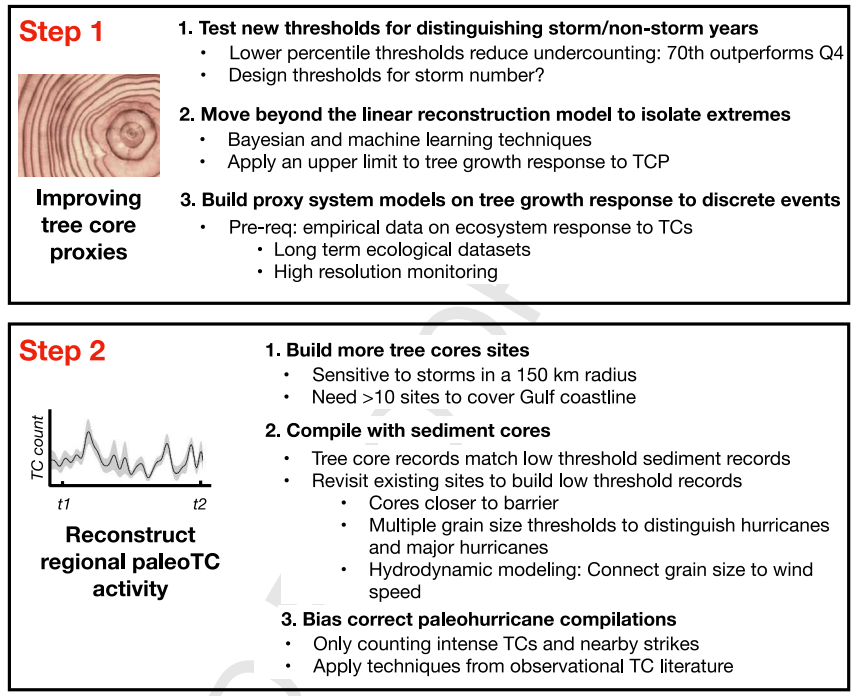

Figure 8. Summary of suggestions for future work aimed at improving tree core proxies of paleohurricane activity and building regional compilations of both tree and sediment core proxies.

Using a fourth quantile threshold on latewood width or reconstructed precipitation amount successfully distinguishes between daily background precipitation and TCP (Figure 6) but proves to be a conservative cutoff for translating TCP to frequency. Across our 1,000 pseudo records, approximately 27% of years with storms over the past millennium are missed with a Q4 threshold. Using a 70th percentile threshold substantially reduces the undercounting of years with at least one storm in our pseudo records (only 12% of years with storms are missed). In addition, a 70th percentile threshold does not overcount storms. Out of 1,000 pseudo records of the past millennium, we only find one year in one record where the 70th percentile threshold counts a year without a storm as having one occur. Below a 70th percentile threshold, we find a substantial loss in the skill of distinguishing between storm years and non-storm years (Figure S2 in Supporting Information S1). Therefore, we recommend that future tree ring records use a 70th percentile threshold to distinguish between TC and non-TC precipitation.

We also tested whether it is possible to establish a threshold that picks out the number of storms that occurred in each year. Given the wide variety of precipitation amounts that can occur in a single storm, we were not able to use a percentile threshold approach to distinguish the number of storms occurring in each year (Figure 2b). A 99th percentile threshold identifies 67% of years with two or more storms in an average past millennium pseudo record (Figure S2 in Supporting Information S1). We cannot successfully distinguish years with three or more storms from tree ring data alone.

Our pseudo proxy approach also highlights some of the biases in the types of storms captured in tree-ring records. In general, TCs generating Q4 rain events tend to pass slower, move closer to the site and pass on the western side of De Soto National Forest (Figure 7). The bias in tree ring proxies toward recording more proximal passing TCs (within a 150-km radius) implies that we will need an extensive tree ring network along the Gulf Coast to successfully reconstruct the actual number of storms that made landfall in this region over the past millennium. Dividing the U.S. Gulf Coast into ∼150 km segments suggests that we would need at least 10 different long leaf pine records from the Gulf shoreline to provide adequate coverage of landfalling TCs. Currently, we only have one tree ring record of storms from this region (Bregy et al., 2022; Figure 1a).

Fortunately, existing tree ring records can theoretically be combined with sediment records to bolster the paleoTC observing network. Sediment records of past storms are more abundant along the Gulf coastline (Figure 1a). Many of the storm properties that promote paleoclimate signatures in longleaf pine trees are also TC

characteristics that promote overwash and inundation at coastal sediment sites. Lin et al. (2014) characterized storms that inundated coastal barriers along the Florida Gulf Coast using a hydrodynamic model and found that 83% (17%) of storms that generated enough surge to inundate the barrier and likely generate widespread overwash passed to the west (east) of the site. Thus, our pseudo proxy work highlights that many of the biases in storms captured by tree-ring proxies and sediment proxies overlap. Such overlapping biases should make it easier to compile/compare sediment and tree ring proxies, because both proxies count the same types of storms and not separate populations of storms that might experience different responses to climate modes.

Many of the storms that generate peaks in latewood growth in De Soto National Forest also make landfall at hurricane intensity or greater. We find strong correlations ($r = 0.51$) between pseudo tree ring records and low threshold (≥Category 1) pseudo sediment records (Figure 5b). These results suggest that there is promise in compiling low threshold sediment records (e.g., Brandon et al., 2013; Lane et al., 2011) with nearby latewood width records. By contrast, the same cannot be said for high threshold sediment records (≥Category 3). Much less of the variance in all JAS storms and pseudo tree ring records ($r = 0.3$, mean rho from 1,000 records) is captured by high threshold pseudo sediment records (Figure 5b). Unfortunately, most paleohurricane reconstructions from the Gulf Coast are high-threshold records (Figure 1a).

Many sedimentary paleohurricane records are generated by collecting a single core from the depocenter of a coastal basin (D. J. Wallace et al., 2014). Overwash fans, however, start at the barrier, and extend back into a basin (Otvos, 2011). Stronger storms can transport larger grains further away from the barrier (Moore et al., 2007). Low-threshold paleohurricane records either collect cores closer to the barrier to capture overwash fans from lower intensity storms (Rodysill et al., 2020) or apply multiple grain size thresholds to identify both hurricanes and major hurricanes (Brandon et al., 2013; Lane et al., 2011). Adding hydrodynamic modeling and examining of sediment grain size distributions could facilitate efforts to tie certain grain sizes to particular wind speed thresholds (Brandon et al., 2013; Woodruff et al., 2008). To improve storm occurrence estimates and encourage multi-proxy comparisons, researchers should revisit high threshold sites/sediment archives and work to recover low-threshold records.

All the above paleorecord biases should be considered when interpreting existing paleohurricane records and compilation of records. Most paleohurricane proxies will more faithfully reconstruct patterns in intense TCs and individual records will only record proximal passing TC years. To assess regional shifts in TCs, paleoclimate records need to be compiled. In addition, TC proxy biases are similar to known storm observation biases which include undercounting of lower intensity and short duration storms especially early in the record (prior to 1940) (Landsea et al., 2010; Vecchi & Knutson, 2011; Villarini et al., 2011). Future work could consider the feasibility of applying bias correction techniques established using modern TC observations to paleohurricane reconstructions.

Unlike their sediment-based counterparts, tree-ring records are not limited by temporal resolution. Sediment records, which are annually resolved at best, often cannot resolve storm response to high frequency variability like ENSO. Our pseudo latewood records exhibit substantial high frequency variability (particularly in the 3–10-year bands) but very little low frequency variability (Figure 4a). Previous work has shown that ENSO variability modulates TC frequency and precipitation along the North American continent (Khouakhi et al., 2017; Nogueira & Keim, 2010). Our pseudo proxy work suggests that ENSO also modifies frequency and precipitation of TCs that make landfall in De Soto National Forest. This variability is captured by latewood records. Synthetic TC rainfall also shows significant variability in low frequency bands (Figure 4b), yet this low frequency variability in mean annual rainfall is not resolved by latewood records. By combining sediment proxies (which isolate low frequency variability) with tree-ring records (which isolate high frequency variability), future multiproxy efforts may be able to explore both low and high frequency natural climate forcings on past TCs, critical for understanding how both will shape the evolution of TC risk in a changing climate.

There are several caveats inherent to this work. Our study is limited to synthetic storms spun up using a single GCM's climate (MPI-ESM). The lack of archived daily wind data for the past millennium limits the available models that can be used for statistical downscaling. The MPI-ESM model, or any other GCM, likely does not reproduce real word climate due to biases and uncertainties in past external forcing (Brohan et al., 2012; PAGES 2k-PMIP3 group, 2015). While MPI climate creates realistic storm tracks and intensity near De Soto National Forest, the model often produces rainier storms than gauge observations (Figure 3e). These biases prevent

analyses of changes in rain magnitude with time but allow for estimating years when TCs occur using quantile thresholds and analyzing pseudo latewood record spectral properties.

Our work highlights the potential for combining sediment records from coastal basins along the Gulf Coast with latewood records from longleaf pine. However, we here only explored one type of tree ring record in one geographic location (Bregy et al., 2022). Recent work has also produced longleaf pine records of TCP in the Carolinas (Maxwell et al., 2021). Further work characterizing how the properties of storms that produce rainy events change along different coastlines will facilitate sensor placement optimization, pinpointing the best sites for multiproxy comparison. In the Gulf of Mexico, storms often make landfall moving perpendicular to the shoreline (Figure 3b); along the US East Coast, storms often move parallel to the coastline (facing northeast) with their front left quadrant impacting coastal tree sites. Storms moving parallel to the shoreline may produce less surge on northeast-facing shorelines of the U.S., making it more difficult to compare tree-ring sites from the Carolinas to coastal sediment records.

As more tree core proxies of extreme rainfall are developed, researchers should test how well different types of reconstruction models represent extremes in precipitation. The linear reconstruction model used for the De Soto National Forest longleaf pine record (Bregy et al., 2022) may not be the best method of reconstructing TCP. Linear models bias results toward the mean and limit our ability to reconstruct extremely rainy storm years. Indeed, the De Soto reconstruction model only captures 40% of the variance in TCP (Bregy et al., 2022). Recent advances in Bayesian techniques (e.g., Itter et al., 2017; Schofield et al., 2016) and machine learning algorithms (e.g., Jevšenak et al., 2018; Salehnia & Ahn, 2022) offer opportunities to build reconstruction models that better fit extreme precipitation data. The use of a linear reconstruction model in this work also allows for ring width to increase indefinitely with rainfall. More work needs to be done exploring if/when there is a cap on latewood growth in longleaf pine such that more rainfall does not equal more tree ring growth. Applying such an upper limit on latewood growth might help resolve the differences in variance between our pseudo latewood records and actual data (Figure 1c).

Finally, the pseudo proxy work presented here represents the first data-model comparison effort for tree-ring records of paleohurricanes. Most existing proxy system models (e.g., Vaganov–Shashkin-Lite (VS-Lite); Tolwinski-Ward et al., 2011) for dendrochronology focus on simulating total ring width in trees. This approach does not allow for explicitly modeling how latewood growth can differ from earlywood growth in response to extreme events. We explored the influence of TCP on annual tree growth using VS-Lite (Tolwinski-Ward et al., 2011) to generate pseudo estimates of total ring width (TW) in De Soto National Forest (Text S2 in Supporting Information S1). Our work shows that using background monthly precipitation in a proxy system model like VS-Lite cannot produce realistic total ring width values in longleaf pine from De Soto National Forest (Figure S3a in Supporting Information S1). Only by including precipitation from extreme weather events (namely TCs) in VS-Lite were we able to produce realistic TW values (Figure S3b in Supporting Information S1). Our VS-Lite results suggest a critical need to build proxy system models that can analyze tree growth response to discrete events like TCs. To build these proxy system models, we need more empirical data on the response of ecosystems to TCs (Pruitt et al., 2019) including high-resolution monitoring before/during/after storms and analysis of extreme event response in long term ecological data sets (e.g., Mitchell et al., 2020; Patrick et al., 2022; Rother et al., 2018). Moreover, addressing this is essential to understanding how longleaf pine forests will respond to changes in the TC hydroclimate incurred by the current warming trend.

5. Conclusions

Understanding the signatures of TC rainfall and occurrence in growth bands in tree rings is a necessary step toward interpreting dendro-based records of hurricane activity. There has been an explosion of tree-ring-based paleohurricane proxies in the last decade (e.g., Maxwell et al., 2021; Trouet et al., 2016; Tucker et al., 2022), and this new proxy type is filling in key gaps in our sediment-based proxy network (e.g., E. J. Wallace, Dee, et al., 2021). It is thus important to combine these two types of paleohurricane proxies, but to date, uncertainties surrounding merging disparate proxy types have not been tested in a pseudo-proxy approach.

To close this gap, we generated pseudo proxies of latewood tree-ring records and sediment records from the U.S. Gulf Coast. We showed that applying traditional quantile thresholds (i.e., Q4-fourth quantile) to latewood data successfully captures most of the variance in storm frequency. This conversion from extremes in latewood growth to TC frequency suggests future multiproxy compilations will be possible. Synthetic TCs recorded in pseudo

latewood records tend to pass close to a site (within 100–150 km), often on the westward side, and have smaller translational velocities (Figure 7). These biases match those found in sediment proxies from the Gulf Coast (Lin et al., 2014) allowing for multi-proxy compilations that capture the same population of storms.

More sediment proxies recovering low-intensity storms (≥Category 1) are needed from the coastline to make future multi-proxy compilations possible. Our work shows there is strong covariance between low-threshold sediment records and tree-ring records (Figure 5), but the strong relationship breaks down for high threshold records, which make up most existing sediment records from the Gulf Coast (Figure 1a). Therefore, we recommend that future efforts focus on returning to existing paleohurricane sites in the Gulf and producing low-threshold records from these basins.

Tree-ring records allow for the reconstruction of high-frequency changes in paleoTCs. Our pseudo records exhibit significant spectral peaks in the ENSO 3–7-year bands suggesting that storm rainfall is modulated by ENSO on interannual timescales (Figure 4). Low-frequency variability, on the other hand, is not captured by tree ring records. By combining sediment and tree-ring records, we can resolve low- and high-frequency changes in TC frequency over the past millennium. This work offers insights generated in a constrained pseudo-proxy test environment providing strong motivation for scientists to compile and compare existing sediment proxies and tree-ring proxies and offers a theoretical approach for doing so. By building multi-proxy compilations of paleostorms, we can help offer insights into long-term TC climate relationships and better constrain TC risk to coastal communities under ongoing global climate changes.

Data Availability Statement

The synthetic storm data and MATLAB scripts for processing is available on Zenodo (Wallace et al., 2024).

Acknowledgments
This work was funded by the National Science Foundation Grant P2C2-2234815 (to E. J. Wallace K. A. Emanuel and S. G. Dee). E. J. Wallace acknowledges support from the Pan Postdoctoral and Rice Academy fellowships at Rice University. Additional funding was provided by NSF P2C2 AGS-2102888 (awarded to Dr. Justin T. Maxwell, with J. C. Bregy funded as a postdoctoral researcher).

References

Ault, T. R., Cole, J. E., Overpeck, J. T., Pederson, G. T., St. George, S., Otto-Bliesner, B., et al. (2013). The continuum of hydroclimate variability in western North America during the last millennium. *Journal of Climate*, *26*(16), 5863–5878. https://doi.org/10.1175/JCLI-D-11-00732.1

Bhatia, K., Vecchi, G., Murakami, H., Underwood, S., & Kossin, J. (2018). Projected response of tropical cyclone intensity and intensification in a global climate model. *Journal of Climate*, *31*(20), 8281–8303. https://doi.org/10.1175/JCLI-D-17-0898.1

Blake, E. S., & Zelinsky, D. A. (2018). *National hurricane center tropical cyclone: Hurricane Harvey (AL092017)*. NOAA National Weather Service.

Brandon, C. M., Woodruff, J. D., Lane, D. P., & Donnelly, J. P. (2013). Tropical cyclone wind speed constraints from resultant storm surge deposition: A 2500 year reconstruction of hurricane activity from St. Marks, FL. *Geochemistry, Geophysics, Geosystems*, *14*(8), 2993–3008. https://doi.org/10.1002/ggge.20217

Bregy, J. C., Maxwell, J. T., Robeson, S. M., Harley, G. L., Elliott, E. A., & Heeter, K. J. (2022). US Gulf Coast tropical cyclone precipitation influenced by volcanism and the North Atlantic subtropical high. *Communications Earth & Environment*, *3*(1), 164. https://doi.org/10.1038/s43247-022-00494-7

Bregy, J. C., Maxwell, J. T., Robeson, S. M., Ortegren, J. T., Soulé, P. T., & Knapp, P. A. (2020). Spatiotemporal variability of tropical cyclone precipitation using a high-resolution, gridded (0.25° × 0.25°) dataset for the eastern United States, 1948–2015. *Journal of Climate*, *33*(5), 1803–1819. https://doi.org/10.1175/JCLI-D-18-0885.1

Bregy, J. C., Wallace, D. J., Minzoni, R. T., & Cruz, V. J. (2018). 2500-year paleotempestological record of intense storms for the northern Gulf of Mexico, United States. *Marine Geology*, *396*, 26–42. https://doi.org/10.1016/j.margeo.2017.09.009

Brohan, P., Allan, R., Freeman, E., Wheeler, D., Wilkinson, C., & Williamson, F. (2012). Constraining the temperature history of the past millennium using early instrumental observations. *Climate of the Past*, *8*(5), 1551–1563. https://doi.org/10.5194/cp-8-1551-2012

Burpee, R. W., & Black, M. L. (1989). Temporal and spatial variations of rainfall near the centers of two tropical cyclones. *Monthly Weather Review*, *117*(10), 2204–2218. https://doi.org/10.1175/1520-0493(1989)117<2204:TASVOR>2.0.CO;2

Cook, E. R., & Peters, K. (1981). The smoothing spline: A new approach to standardizing forest interior tree-ring width series for dendroclimatic studies. *Tree-Ring Bulletin*, *41*, 45–53.

Czajkowski, J., Villarini, G., Montgomery, M., Michel-Kerjan, E., & Goska, R. (2017). Assessing current and future freshwater flood risk from North Atlantic tropical cyclones via insurance claims. *Scientific Reports*, *7*(1), 41609. https://doi.org/10.1038/srep41609

Dare, R. A., & McBride, J. L. (2011). The threshold sea surface temperature condition for tropical cyclogenesis. *Journal of Climate*, *24*(17), 4570–4576. https://doi.org/10.1175/JCLI-D-10-05006.1

Dee, S., Emile-Geay, J., Evans, M. N., Allam, A., Steig, E. J., & Thompson, D. M. (2015). PRYSM: An open-source framework for PRoxY system modeling, with applications to oxygen-isotope systems: PRYSM: Proxy system modeling. *Journal of Advances in Modeling Earth Systems*, *7*(3), 1220–1247. https://doi.org/10.1002/2015MS000447

Diaz, H. F., & Pulwarty, R. S. (1994). An analysis of the time scales of variability in centuries-long ENSO-sensitive records in the last 1000 years. *Climate Change*, *26*(2–3), 317–342. https://doi.org/10.1007/bf01092422

Didlake, A. C., & Kumjian, M. R. (2018). Examining storm asymmetries in hurricane irma (2017) using polarimetric radar observations. *Geophysical Research Letters*, *45*(24). https://doi.org/10.1029/2018GL080739

Donnelly, J. P., Hawkes, A. D., Lane, P., Macdonald, D., Shuman, B. N., Toomey, M. R., et al. (2015). Climate forcing of unprecedented intense-hurricane activity in the last 2000 years. *Earth's Future*, *3*(2), 49–65. https://doi.org/10.1002/2014EF000274

Donnelly, J. P., & Woodruff, J. D. (2007). Intense hurricane activity over the past 5,000 years controlled by El Niño and the West African monsoon. *Nature*, *447*(7143), 465–468. https://doi.org/10.1038/nature05834

Emanuel, K. (1999). Thermodynamic control of hurricane intensity. *Nature*, *401*(6754), 665–669. https://doi.org/10.1038/44326
Emanuel, K. (2003). Tropical cyclones. *Annual Review of Earth and Planetary Sciences*, *31*(1), 75–104. https://doi.org/10.1146/annurev.earth.31.100901.141259
Emanuel, K. (2017). Assessing the present and future probability of Hurricane Harvey's rainfall. *Proceedings of the National Academy of Sciences*, *114*(48), 12681–12684. https://doi.org/10.1073/pnas.1716222114
Emanuel, K., Sundararajan, R., & Williams, J. (2008). Hurricanes and global warming: Results from downscaling IPCC AR4 simulations. *Bulletin of the American Meteorological Society*, *89*(3), 347–367. https://doi.org/10.1175/BAMS-89-3-347
Ensor, L. A., & Robeson, S. M. (2008). Statistical characteristics of daily precipitation: Comparisons of gridded and point datasets. *Journal of Applied Meteorology and Climatology*, *47*(9), 2468–2476. https://doi.org/10.1175/2008JAMC1757.1
Evans, M. N., Tolwinski-Ward, S. E., Thompson, D. M., & Anchukaitis, K. J. (2013). Applications of proxy system modeling in high resolution paleoclimatology. *Quaternary Science Reviews*, *76*, 16–28. https://doi.org/10.1016/j.quascirev.2013.05.024
Feldmann, M., Emanuel, K., Zhu, L., & Lohmann, U. (2019). Estimation of Atlantic tropical cyclone rainfall frequency in the United States. *Journal of Applied Meteorology and Climatology*, *58*(8), 1853–1866. https://doi.org/10.1175/JAMC-D-19-0011.1
Giorgetta, M. A., Jungclaus, J., Reick, C. H., Legutke, S., Bader, J., Böttinger, M., et al. (2013). Climate and carbon cycle changes from 1850 to 2100 in MPI-ESM simulations for the Coupled Model Intercomparison Project phase 5. *Journal of Advances in Modeling Earth Systems*, *5*(3), 572–597. https://doi.org/10.1002/jame.20038
Gray, W. M. (1984). Atlantic seasonal hurricane frequency. Part I: El Niño and 30 mb Quasi-Biennial Oscillation influences. *Monthly Weather Review*, *112*(9), 1649–1668. https://doi.org/10.1175/1520-0493(1984)112<1649:ASHFPI>2.0.CO;2
Guzman, O., & Jiang, H. (2021). Global increase in tropical cyclone rain rate. *Nature Communications*, *12*(1), 5344. https://doi.org/10.1038/s41467-021-25685-2
Hall, T. M., & Kossin, J. P. (2019). Hurricane stalling along the North American coast and implications for rainfall. *Npj Climate and Atmospheric Science*, *2*(1), 17. https://doi.org/10.1038/s41612-019-0074-8
Higgins, R. W., Shi, W., Yarosh, E., & Joyce, R. (2000). *Improved United States precipitation quality control system and analysis (NCEP/Climate Prediction Center ATLAS 7)* (p. 40). National Oceanic and Atmospheric Administration.
Horton, B. P., Rossi, V., & Hawkes, A. D. (2009). The sedimentary record of the 2005 hurricane season from the Mississippi and Alabama coastlines. *Quaternary International*, *195*(1–2), 15–30. https://doi.org/10.1016/j.quaint.2008.03.004
Itter, M. S., Finley, A. O., D'Amato, A. W., Foster, J. R., & Bradford, J. B. (2017). Variable effects of climate on forest growth in relation to climate extremes, disturbance, and forest dynamics. *Ecological Applications*, *27*(4), 1082–1095. https://doi.org/10.1002/eap.1518
Jevšenak, J., Džeroski, S., Zavadlav, S., & Levanič, T. (2018). A machine learning approach to analyzing the relationship between temperatures and multi-proxy tree-ring records. *Tree-Ring Research*, *74*(2), 210–224. https://doi.org/10.3959/1536-1098-74.2.210
Khouakhi, A., Villarini, G., & Vecchi, G. A. (2017). Contribution of tropical cyclones to rainfall at the global scale. *Journal of Climate*, *30*(1), 359–372. https://doi.org/10.1175/JCLI-D-16-0298.1
Klotzbach, P. J., Saunders, M. A., Bell, G. D., & Blake, E. S. (2017). North Atlantic seasonal hurricane prediction: Underlying science and an evaluation of statistical models. In S.-Y. S. Wang, J.-H. Yoon, C. C. Funk, & R. R. Gillies (Eds.), *Geophysical monograph series* (pp. 315–328). John Wiley & Sons, Inc. https://doi.org/10.1002/9781119068020.ch19
Knapp, K., Kruk, M. C., Levinson, D. H., Diamond, H. J., & Neumann, C. J. (2010). The international best track archive for climate stewardship (IBTrACS). *Bulletin of the American Meteorological Society*, *91*(3), 363–376. https://doi.org/10.1175/2009BAMS2755.1
Knapp, P. A., Maxwell, J. T., & Soulé, P. T. (2016). Tropical cyclone rainfall variability in coastal North Carolina derived from longleaf pine (Pinus palustris Mill.): AD 1771–2014. *Climatic Change*, *135*(2), 311–323. https://doi.org/10.1007/s10584-015-1560-6
Knapp, P. A., Soulé, P. T., Maxwell, J. T., Ortegren, J. T., & Mitchell, T. J. (2021). Tropical cyclone precipitation regimes since 1750 and the Great Suppression of 1843–1876 along coastal North Carolina, USA. *International Journal of Climatology*, *41*(1), 200–210. https://doi.org/10.1002/joc.6615
Kossin, J. P., Camargo, S. J., & Sitkowski, M. (2010). Climate modulation of North Atlantic hurricane tracks. *Journal of Climate*, *23*(11), 3057–3076. https://doi.org/10.1175/2010JCLI3497.1
Landsea, C. W., & Franklin, J. L. (2013). Atlantic hurricane database uncertainty and presentation of a new database format. *Monthly Weather Review*, *141*(10), 3576–3592. https://doi.org/10.1175/MWR-D-12-00254.1
Landsea, C. W., Vecchi, G. A., Bengtsson, L., & Knutson, T. R. (2010). Impact of duration thresholds on Atlantic tropical cyclone counts. *Journal of Climate*, *23*(10), 2508–2519. https://doi.org/10.1175/2009JCLI3034.1
Lane, P., Donnelly, J. P., Woodruff, J. D., & Hawkes, A. D. (2011). A decadally-resolved paleohurricane record archived in the late Holocene sediments of a Florida sinkhole. *Marine Geology*, *287*(1–4), 14–30. https://doi.org/10.1016/j.margeo.2011.07.001
Lee, C.-Y., Camargo, S. J., Sobel, A. H., & Tippett, M. K. (2020). Statistical–dynamical downscaling projections of tropical cyclone activity in a warming climate: Two diverging genesis scenarios. *Journal of Climate*, *33*(11), 4815–4834. https://doi.org/10.1175/JCLI-D-19-0452.1
Li, L., & Chakraborty, P. (2020). Slower decay of landfalling hurricanes in a warming world. *Nature*, *587*(7833), 230–234. https://doi.org/10.1038/s41586-020-2867-7
Lin, N., Lane, P., Emanuel, K. A., Sullivan, R. M., & Donnelly, J. P. (2014). Heightened hurricane surge risk in northwest Florida revealed from climatological-hydrodynamic modeling and paleorecord reconstruction. *Journal of Geophysical Research: Atmospheres*, *119*(14), 1–18. https://doi.org/10.1002/2014JD021584
Liu, K., & Fearn, M. L. (1993). Lake-sediment record of late Holocene hurricane. *Geology*, *21*(September), 793–796. https://doi.org/10.1130/0091-7613(1993)021<0793
Liu, K., & Fearn, M. L. (2000). Reconstruction of prehistoric landfall frequencies of catastrophic hurricanes in northwestern Florida from lake sediment records. *Quaternary Research*, *54*(2), 238–245. https://doi.org/10.1006/qres.2000.2166
Liu, K.-B., Li, C., Bianchette, T. A., McCloskey, T. A., Yao, Q., & Weeks, E. (2011). Storm deposition in a coastal backbarrier lake in Louisiana Caused by Hurricanes Gustav and Ike. *Journal of Coastal Research*, 1866–1870.
Lonfat, M., Marks, F. D., & Chen, S. S. (2004). Precipitation distribution in tropical cyclones using the tropical rainfall measuring mission (TRMM) microwave imager: A global perspective. *Monthly Weather Review*, *132*(7), 1645–1660. https://doi.org/10.1175/1520-0493(2004)132<1645:PDITCU>2.0.CO;2
Lu, P., Lin, N., Emanuel, K., Chavas, D., & Smith, J. (2018). Assessing hurricane rainfall mechanisms using a physics-based model: Hurricanes isabel (2003) and irene (2011). *Journal of the Atmospheric Sciences*, *75*(7), 2337–2358. https://doi.org/10.1175/JAS-D-17-0264.1
Matyas, C. J. (2010). Associations between the size of hurricane rain fields at landfall and their surrounding environments. *Meteorology and Atmospheric Physics*, *106*(3–4), 135–148. https://doi.org/10.1007/s00703-009-0056-1

Maxwell, J. T., Bregy, J. C., Robeson, S. M., Knapp, P. A., Soulé, P. T., & Trouet, V. (2021). Recent increases in tropical cyclone precipitation extremes over the US east coast. *Proceedings of the National Academy of Sciences of the United States of America*, *118*(41), e2105636118. https://doi.org/10.1073/pnas.2105636118

Miller, D. L., Mora, C. I., Grissino-Mayer, H. D., Mock, C. J., Uhle, M. E., & Sharp, Z. (2006). Tree-ring isotope records of tropical cyclone activity. *Proceedings of the National Academy of Sciences*, *103*(39), 14294–14297. https://doi.org/10.1073/pnas.0606549103

Mitchell, T. J., Knapp, P. A., & Patterson, T. W. (2020). The importance of infrequent, high-intensity rainfall events for longleaf pine (Pinus palustris Mill.) radial growth and implications for dendroclimatic research. *Trees, Forests and People*, *1*, 100009. https://doi.org/10.1016/j.tfp.2020.100009

Montpellier, E. E., Knapp, P. A., Soulé, P. T., & Maxwell, J. T. (2020). Microelevational differences affect longleaf pine (Pinus palustris Mill.) sensitivity to tropical cyclone precipitation: A case study using lidar. *Tree-Ring Research*, *76*(2), 89. https://doi.org/10.3959/TRR2019-9

Moore, A. L., McAdoo, B. G., & Ruffman, A. (2007). Landward fining from multiple sources in a sand sheet deposited by the 1929 Grand Banks tsunami, Newfoundland. *Sedimentary Geology*, *200*(3–4), 336–346. https://doi.org/10.1016/j.sedgeo.2007.01.012

Nogueira, R. C., & Keim, B. D. (2010). Annual volume and area variations in tropical cyclone rainfall over the eastern United States. *Journal of Climate*, *23*(16), 4363–4374. https://doi.org/10.1175/2010JCLI3443.1

Oliva, F., Viau, A. E., Peros, M. C., & Bouchard, M. (2018). Paleotempestology database for the western North Atlantic basin. *The Holocene*, *28*(10), 1664–1671. https://doi.org/10.1177/0959683618782598

Otvos, E. G. (2011). Hurricane signatures and landforms-toward improved interpretations and global storm climate chronology. *Sedimentary Geology*, *239*(1–2), 10–22. https://doi.org/10.1016/j.sedgeo.2011.04.014

PAGES 2k-PMIP3 group. (2015). Continental-scale temperature variability in PMIP3 simulations and PAGES 2k regional temperature reconstructions over the past millennium. *Climate of the Past*, *11*(12), 1673–1699. https://doi.org/10.5194/cp-11-1673-2015

Patrick, C. J., Kominoski, J. S., McDowell, W. H., Branoff, B., Lagomasino, D., Leon, M., et al. (2022). A general pattern of trade-offs between ecosystem resistance and resilience to tropical cyclones. *Science Advances*, *8*(9), eabl9155. https://doi.org/10.1126/sciadv.abl9155

Patricola, C. M., Saravanan, R., & Chang, P. (2014). The impact of the El Niño–southern Oscillation and Atlantic meridional mode on seasonal Atlantic tropical cyclone activity. *Journal of Climate*, *27*(14), 5311–5328. https://doi.org/10.1175/JCLI-D-13-00687.1

Pielke, R. A., Gratz, J., Landsea, C. W., Collins, D., Saunders, M. A., & Musulin, R. (2008). Normalized hurricane damage in the United States: 1900-2005. *Natural Hazards Review*, *9*(1), 29–42. https://doi.org/10.1061/(asce)1527-6988(2008)9:1(29)

Pruitt, J. N., Little, A. G., Majumdar, S. J., Schoener, T. W., & Fisher, D. N. (2019). Call-to-Action: A global consortium for tropical cyclone ecology. *Trends in Ecology & Evolution*, *34*(7), 588–590. https://doi.org/10.1016/j.tree.2019.04.009

Rappaport, E. N. (2014). Fatalities in the United States from Atlantic tropical cyclones: New data and interpretation. *Bulletin of the American Meteorological Society*, *95*(3), 341–346. https://doi.org/10.1175/BAMS-D-12-00074.1

Reese, C. A., Strange, T. P., Lynch, W. D., & Liu, K. B. (2008). Geologic evidence of hurricane Katrina recovered from the Pearl river Marsh, MS/LA. *Journal of Coastal Research*, *24*(6), 1601–1607. https://doi.org/10.2112/07-0956.1

Risser, M. D., & Wehner, M. F. (2017). Attributable human-induced changes in the likelihood and magnitude of the observed extreme precipitation during hurricane Harvey. *Geophysical Research Letters*, *44*(24), 12–457. https://doi.org/10.1002/2017GL075888

Rodysill, J., Donnelly, J. P., Sullivan, R. M., Lane, P. D., Toomey, M. R., Woodruff, J. D., et al. (2020). Historically unprecedented Northern Gulf of Mexico hurricane activity from 650 to 1250 CE. *Scientific Reports*, *10*, 1–17. https://doi.org/10.1038/s41598-020-75874-0

Rother, M. T., Huffman, J. M., Harley, G. L., Platt, W. J., Jones, N., Robertson, K. M., & Orzell, S. L. (2018). Cambial phenology informs tree-ring analysis of fire seasonality in coastal plain pine savannas. *Fire Ecology*, *14*(1), 164–185. https://doi.org/10.4996/fireecology.140116418

Salehnia, N., & Ahn, J. (2022). Modelling and reconstructing tree ring growth index with climate variables through artificial intelligence and statistical methods. *Ecological Indicators*, *134*, 108496. https://doi.org/10.1016/j.ecolind.2021.108496

Schmitt, D., Gischler, E., Anselmetti, F. S., & Vogel, H. (2020). Caribbean cyclone activity: An annually-resolved Common Era record. *Scientific Reports*, *10*, 1–17. https://doi.org/10.1038/s41598-020-68633-8

Schofield, M. R., Barker, R. J., Gelman, A., Cook, E. R., & Briffa, K. R. (2016). A model-based approach to climate reconstruction using tree-ring data. *Journal of the American Statistical Association*, *111*(513), 93–106. https://doi.org/10.1080/01621459.2015.1110524

Sobel, A. H., Wing, A. A., Camargo, S. J., Patricola, C. M., Vecchi, G. A., Lee, C. Y., & Tippett, M. K. (2021). Tropical cyclone frequency. *Earth's Future*, *9*(12), 1–34. https://doi.org/10.1029/2021EF002275

Sugi, M., Murakami, H., & Yoshida, K. (2017). Projection of future changes in the frequency of intense tropical cyclones. *Climate Dynamics*, *49*(1–2), 619–632. https://doi.org/10.1007/s00382-016-3361-7

Terry, J. P., & Feng, C.-C. (2010). On quantifying the sinuosity of typhoon tracks in the western North Pacific basin. *Applied Geography*, *30*(4), 678–686. https://doi.org/10.1016/j.apgeog.2010.01.007

Thomson, D. J. (1982). Spectrum estimation and harmonic analysis. *Proceedings of the IEEE*, *70*(9), 1055–1096. https://doi.org/10.1109/PROC.1982.12433

Tolwinski-Ward, S. E., Evans, M. N., Hughes, M. K., & Anchukaitis, K. J. (2011). An efficient forward model of the climate controls on interannual variation in tree-ring width. *Climate Dynamics*, *36*(11–12), 2419–2439. https://doi.org/10.1007/s00382-010-0945-5

Touma, D., Stevenson, S., Camargo, S. J., Horton, D. E., & Diffenbaugh, N. S. (2019). Variations in the intensity and spatial extent of tropical cyclone precipitation. *Geophysical Research Letters*, *46*(23), 13992–14002. https://doi.org/10.1029/2019GL083452

Trouet, V., Harley, G. L., & Domínguez-Delmás, M. (2016). Shipwreck rates reveal Caribbean tropical cyclone response to past radiative forcing. *Proceedings of the National Academy of Sciences*, *113*(12), 3169–3174. https://doi.org/10.1073/pnas.1519566113

Tu, S., Xu, J., Chan, J. C. L., Huang, K., Xu, F., & Chiu, L. S. (2021). Recent global decrease in the inner-core rain rate of tropical cyclones. *Nature Communications*, *12*(1), 1948. https://doi.org/10.1038/s41467-021-22304-y

Tucker, C. S., & Pearl, J. K. (2021). Coastal tree-ring records for paleoclimate and paleoenvironmental applications in North America. *Quaternary Science Reviews*, *265*, 107044. https://doi.org/10.1016/j.quascirev.2021.107044

Tucker, C. S., Pearl, J. K., Elliott, E. A., Bregy, J. C., Friedman, J. M., & Therrell, M. D. (2022). Baldcypress false ring formation linked to summer hydroclimatic extremes in the southeastern United States. *Environmental Research Letters*, *17*(11), 114030. https://doi.org/10.1088/1748-9326/ac9745

Van Oldenborgh, G. J., Van Der Wiel, K., Sebastian, A., Singh, R., Arrighi, J., Otto, F., et al. (2017). Attribution of extreme rainfall from hurricane Harvey, august 2017. *Environmental Research Letters*, *12*(12), 124009. https://doi.org/10.1088/1748-9326/aa9ef2

Vecchi, G. A., & Knutson, T. R. (2011). Estimating annual numbers of Atlantic hurricanes missing from the HURDAT database (1878-1965) using ship track density. *Journal of Climate*, *24*(6), 1736–1746. https://doi.org/10.1175/2010JCLI3810.1

Villarini, G., Vecchi, G. A., Knutson, T. R., & Smith, J. A. (2011). Is the recorded increase in short-duration North Atlantic tropical storms spurious? *Journal of Geophysical Research*, *116*(D10114), 1–11. https://doi.org/10.1029/2010JD015493

Wallace, D. J., Woodruff, J. D., Anderson, J. B., & Donnelly, J. P. (2014). Palaeohurricane reconstructions from sedimentary archives along the Gulf of Mexico, caribbean sea and western North Atlantic ocean margins. *Sedimentary Coastal Zones from High to Low Latitudes: Similarities and Differences*, *388*(1), 481–501. https://doi.org/10.1144/SP388.12

Wallace, E., Bregy, J., Dee, S., & Emanuel, K. (2024). Building pseudo latewood tree ring records for De Soto National Forest using MPI-ESM synthetic storms for the past millennium [Dataset]. *Paleoceanography & Paleoclimatology*. Zenodo. https://doi.org/10.5281/zenodo.12547725

Wallace, E. J., Coats, S., Emanuel, K. A., & Donnelly, J. P. (2020). Centennial-scale shifts in storm frequency captured in paleohurricane records from the Bahamas arise predominantly from random variability. *Geophysical Research Letters*, *48*(1). https://doi.org/10.1029/2020GL091145

Wallace, E. J., & Dee, S. G. (2022). Tropical cyclone frequency: Turning paleoclimate into projections. *Environmental Research: Climate*, *1*(2), 023002. https://doi.org/10.1088/2752-5295/aca785

Wallace, E. J., Dee, S. G., & Emanuel, K. A. (2021a). Resolving long-term variations in North Atlantic tropical cyclone activity using a pseudo proxy paleotempestology network approach. *Geophysical Research Letters*, *48*(18), 1–13. https://doi.org/10.1029/2021gl094891

Wallace, E. J., Donnelly, J. P., van Hengstum, P. J., Wiman, C., Sullivan, R. M., Winkler, T. S., et al. (2019). Intense hurricane activity over the past 1500 years at South Andros Island, the Bahamas. *Paleoceanography and Paleoclimatology*, *34*(11), 1761–1783. https://doi.org/10.1029/2019PA003665

Wallace, E. J., Donnelly, J. P., van Hengstum, P. J., Winkler, T. S., Dizon, C., LaBella, A., et al. (2021b). Regional shifts in paleohurricane activity over the last 1500 years derived from blue hole sediments offshore of Middle Caicos Island. *Quaternary Science Reviews*, *268*, 1–18. https://doi.org/10.1016/j.quascirev.2021.107126

Wallace, E. J., Donnelly, J. P., van Hengstum, P. J., Winkler, T. S., McKeon, K., Macdonald, D., et al. (2021c). 1050 years of hurricane strikes on Long Island in the Bahamas. *Paleoceanography and Paleoclimatology*, *36*(3). https://doi.org/10.1029/2020PA004156

Williams, H. F. L. (2013). 600-year sedimentary archive of hurricane strikes in a prograding beach ridge plain, southwestern Louisiana. *Marine Geology*, *336*, 170–183. https://doi.org/10.1016/j.margeo.2012.12.005

Winkler, T. S., van Hengstum, P. J., Donnelly, J. P., Wallace, E. J., D'Entrement, N. E., Hawkes, A. D., et al. (2022). Oceanic passage of hurricanes across Cay Sal Bank in the Bahamas over the last 600 years. *Marine Geology*, *443*(3), 106653. https://doi.org/10.1016/j.margeo.2021.106653

Winkler, T. S., Van Hengstum, P. J., Donnelly, J. P., Wallace, E. J., Sullivan, R. M., Macdonald, D., & Albury, N. A. (2020). Revising evidence of hurricane strikes on Abaco Island (The Bahamas) over the last 680 years. *Scientific Reports*, *10*(1), 16556. https://doi.org/10.1038/s41598-020-73132-x

Woodruff, J. D., Donnelly, J. P., Mohrig, D., & Geyer, W. R. (2008). Reconstructing relative flooding intensities responsible for hurricane-induced deposits from Laguna Playa Grande, Vieques, Puerto Rico. *Geology*, *36*(5), 391–394. https://doi.org/10.1130/G24731A.1

Yang, W., Wallace, E., Vecchi, G. A., Donnelly, J. P., Emile-Geay, J., Hakim, G. J., et al. (2024). Last millennium hurricane activity linked to endogenous climate variability. *Nature Communications*, *15*(1), 816. https://doi.org/10.1038/s41467-024-45112-6

Yu, Z., Wang, Y., Xu, H., Davidson, N., Chen, Y., Chen, Y., & Yu, H. (2017). On the relationship between intensity and rainfall distribution in tropical cyclones making landfall over China. *Journal of Applied Meteorology and Climatology*, *56*(10), 2883–2901. https://doi.org/10.1175/JAMC-D-16-0334.1

Zhu, L., Quiring, S. M., & Emanuel, K. A. (2013). Estimating tropical cyclone precipitation risk in Texas. *Geophysical Research Letters*, *40*(23), 6225–6230. https://doi.org/10.1002/2013GL058284

References From the Supporting Information

Cook, E. R., & Holmes, R. (1986). *Users manual for program ARSTAN*. University of Arizona Laboratory of Tree-Ring Research.

Emanuel, K. (2006). Climate and tropical cyclone activity: A new model downscaling approach. *Journal of Climate*, *19*(October), 4797–4802. https://doi.org/10.1175/jcli3908.1

Emanuel, K., DesAutels, C., Holloway, C., & Korty, R. (2004). Environmental control of tropical cyclone intensity. *Journal of the Atmospheric Sciences*, *61*(7), 843–858. https://doi.org/10.1175/1520-0469(2004)061<0843:ECOTCI>2.0.CO;2

Emanuel, K., Ravela, S., Vivant, E., & Risi, C. (2006). A statistical deterministic approach to hurricane risk assessment. *Bulletin of the American Meteorological Society*, *87*(3), 299–314. https://doi.org/10.1175/BAMS-87-3-299

Emanuel, K., & Rotunno, R. (2011). Self-stratification of tropical cyclone outflow. Part I: Implications for storm structure. *Journal of the Atmospheric Sciences*, *68*(10), 2236–2249. https://doi.org/10.1175/JAS-D-10-05024.1

Hawkins, E., Osborne, T. M., Ho, C. K., & Challinor, A. J. (2013). Calibration and bias correction of climate projections for crop modelling: An idealised case study over Europe. *Agricultural and Forest Meteorology*, *170*, 19–31. https://doi.org/10.1016/j.agrformet.2012.04.007

Higgins, R. W., Silva, V. B. S., Kousky, V. E., & Shi, W. (2008). Comparison of daily precipitation statistics for the United States in observations and in the NCEP climate forecast system. *Journal of Climate*, *21*(22), 5993–6014. https://doi.org/10.1175/2008JCLI2339.1

Huang, J., Van Den Dool, H., & Georgakakos, K. (1996). Analysis of model-calculated soil moisture over the United States (1931–1993) and applications to long-range temperature forecasts. *Journal of Climate*, *9*(6), 1350–1362. https://doi.org/10.1175/1520-0442(1996)009<1350:aomcsm>2.0.co;2

Jungclaus, J. H., Fischer, N., Haak, H., Lohmann, K., Marotzke, J., Matei, D., et al. (2013). Characteristics of the ocean simulations in the Max Planck Institute Ocean Model (MPIOM) the ocean component of the MPI-Earth system model. *Journal of Advances in Modeling Earth Systems*, *5*(2), 422–446. https://doi.org/10.1002/jame.20023

Kistler, R., Kalnay, E., Collins, W., Saha, S., White, G., Woollen, J., et al. (2001). The NCEP-NCAR 50-year reanalysis: Monthly means CD-ROM and documentation. *Bulletin of the American Meteorological Society*, *82*(2), 247–267. https://doi.org/10.1175/1520-0477(2001)082<0247:TNNYRM>2.3.CO;2

Reick, C. H., Raddatz, T., Brovkin, V., & Gayler, V. (2013). Representation of natural and anthropogenic land cover change in MPI-ESM. *Journal of Advances in Modeling Earth Systems*, *5*(3), 459–482. https://doi.org/10.1002/jame.20022

Schneck, R., Reick, C. H., & Raddatz, T. (2013). Land contribution to natural CO_2 variability on time scales of centuries. *Journal of Advances in Modeling Earth Systems*, *5*(2), 354–365. https://doi.org/10.1002/jame.20029

Stevens, B., Giorgetta, M., Esch, M., Mauritsen, T., Crueger, T., Rast, S., et al. (2013). Atmospheric component of the MPI-M earth system model: ECHAM6. *Journal of Advances in Modeling Earth Systems*, *5*(2), 146–172. https://doi.org/10.1002/jame.20015

Tolwinski-Ward, S. E., Anchukaitis, K. J., & Evans, M. N. (2013). Bayesian parameter estimation and interpretation for an intermediate model of tree-ring width. *Climate of the Past*, *9*(4), 1481–1493. https://doi.org/10.5194/cp-9-1481-2013